

The Initial Mass Function of Low-Mass Stars and Brown Dwarfs in Taurus¹

K. L. Luhman

Harvard-Smithsonian Center for Astrophysics, 60 Garden St., Cambridge, MA 02138

kluhman@cfa.harvard.edu

ABSTRACT

By combining deep optical imaging and infrared spectroscopy with data from the Two-Micron All-Sky Survey (2MASS) and from previous studies (e.g., Briceño et al.), I have measured the Initial Mass Function (IMF) for a reddening-limited sample in four fields in the Taurus star forming region. This IMF is representative of the young populations within these fields for masses above $0.02 M_{\odot}$. Relative to the similarly derived IMF for the Trapezium Cluster (Luhman et al.), the IMF for Taurus exhibits a modest deficit of stars above one solar mass (i.e., steeper slope), the same turnover mass ($\sim 0.8 M_{\odot}$), and a significant deficit of brown dwarfs. If the IMF in Taurus were the same as that in the Trapezium, 12.8 ± 1.8 brown dwarfs ($> 0.02 M_{\odot}$) are expected in these Taurus fields where only one brown dwarf candidate is found. These results are used to test theories of the IMF.

Subject headings: infrared: stars — stars: evolution — stars: formation — stars: low-mass, brown dwarfs — stars: luminosity function, mass function — stars: pre-main sequence

1. Introduction

A great deal of insight into the process of star formation can be gained by measuring the initial mass function (IMF) of low-mass stars and brown dwarfs. The presence of a flattening or turnover in the IMF, the value of such a characteristic mass, the shape of the IMF into the substellar regime, the minimum mass at which objects form in isolation, and the variation of these properties with environmental conditions can provide discriminating tests of the wide range of theories for how the masses of stars are determined.

¹Visiting Astronomer, Kitt Peak National Observatory, National Optical Astronomy Observatories, which is operated by the Association of Universities for Research in Astronomy, Inc. (AURA) under cooperative agreement with the National Science Foundation.

In an effort to measure accurately and precisely the low-mass IMF under a wide range of conditions, the populations within the nearby star forming clusters IC 348 (Luhman et al. 1998b), ρ Oph (Luhman & Rieke 1999), and the Trapezium Cluster (Luhman et al. 2000) were studied in detail. As summarized by Luhman et al. (2000), the stellar IMFs in these clusters were found to be similar over a wide range of stellar densities (ρ Oph, $n = 0.2\text{-}1 \times 10^3 \text{ pc}^{-3}$; IC 348, $n = 1 \times 10^3 \text{ pc}^{-3}$; Trapezium, $n = 1\text{-}5 \times 10^4 \text{ pc}^{-3}$), while modest variations in the substellar IMFs were not ruled out. The data for star forming clusters (see also Hillenbrand & Carpenter 2000), young open clusters (Bouvier et al. 1998; Barrado y Navascués et al. 2000), and the field (Reid et al. 1999) were shown to be consistent with the same IMF, one that is flat or rises slowly from the substellar regime to about $0.6 M_{\odot}$, and then rolls over into a power law that continues from about $1 M_{\odot}$ to higher masses, consistent the notion that the majority of field stars were born in clusters (Lada, Strom, & Myers 1993). Meanwhile, a different IMF characterizes Galactic globular clusters (Paresce & De Marchi 2000), one that can be described by a log-normal form with a characteristic mass of $0.33 M_{\odot}$. These studies of star forming and open clusters, the field, and globular clusters represent the most reliable measurements of the low-mass IMF to date. The observed variation in the IMF from the field and Galactic clusters to globular clusters motivates further studies of the low-mass IMF under a greater variety of environments.

Whereas the young stellar populations from the previous studies represent the clustered mode of star formation ($n = 10^2\text{-}10^4 \text{ pc}^{-3}$), the stars in the Taurus-Auriga molecular cloud are forming in relative isolation ($1\text{-}10 \text{ pc}^{-3}$). Because of the compact nature of star forming clusters, candidate members can be efficiently identified through optical and infrared (IR) imaging and confirmed through multi-object spectroscopy. The completeness limits in mass and reddening of such samples are easily defined with IR photometry, which is essential for a measurement of the IMF (see, e.g., Luhman et al. 2000). In contrast, the population in the Taurus star forming region is spread across a much larger area of sky, dramatically increasing the field star contamination and reducing the observing efficiency. Consequently, unlike the unbiased samples defined for clusters, young stars in Taurus are usually identified through specific selection criteria (e.g., emission in $\text{H}\alpha$, X-rays, or the far-IR). Such samples are not satisfactory for measurements of the IMF because the biases and mass completeness limits are not readily quantified.

In a few recent studies, representative measurements of the low-mass population in Taurus have been attempted. Strom & Strom (1994) and Luhman & Rieke (1998) (hereafter LR98) used optical and IR imaging and spectroscopy to estimate the IMF in L1495, one of the more well-defined stellar aggregates in Taurus. To search for objects at lower masses over a larger area, Briceño et al. (1998) (hereafter BHSM) obtained RI imaging of the L1495, B209, L1529, and L1551 dark clouds. Because of the proximity and youth of Taurus, the locus of members in the BHSM optical color-magnitude diagram was well-separated from most of the background population. BHSM obtained spectroscopy of candidate low-mass members to search for signatures of youth and membership, such as Li absorption, strong $\text{H}\alpha$ emission, and pre-main-sequence spectral features. Although their observations were sensitive to unreddened young brown dwarfs with masses of $\gtrsim 0.03 M_{\odot}$ (M8-

M9), they found objects down to only $\sim 0.08 M_{\odot}$ (M6-M6.5). However, because the observations were conducted in the optical and the members become redder with later types, the survey was complete to progressively lower levels of extinction with decreasing mass. Consequently, it was unclear whether the absence of brown dwarfs in the BHSM study was statistically significant.

To measure an IMF for Taurus that is representative at masses of $\gtrsim 0.02 M_{\odot}$, I have obtained spectroscopy of low-mass candidates identified by LR98 and have searched for brown dwarfs at low masses and moderately high reddenings by combining deep I and z' imaging of the BHSM fields with IR photometry from the Two-Micron All-Sky Survey (2MASS). The techniques employed by Luhman et al. (2000) and references therein are used to calculate the IMF for this area. The Taurus IMF is found to have the same shape as the Trapezium IMF from 0.1-1 M_{\odot} , but with moderately fewer stars above 1 M_{\odot} and a significant deficit of brown dwarfs. The implications of these results for theories of the IMF are discussed.

2. Observations and Data Analysis

2.1. Spectroscopy

I selected for IR spectroscopy 16 of the 17 low-mass candidates identified by LR98 in JK_s imaging of a $10' \times 10'$ field towards the area of highest extinction in the L1495 dark cloud. Additional spectra were obtained for the dwarf spectral type standards GL 382 (M2V), GL 381 (M2.5V), GL 51 (M5V), LHS 2243 (M8V), LHS 2065 (M9V), BRI 0021-0214 (\geq M9.5), and 2MASP J0345432+254023 (L0V) and the optically-classified pre-main-sequence sources V410 X-ray 3 (M6), 5a (M5.5), and 6 (M5.5). The observations were performed with the near-IR long-slit spectrometer CRSP at the Kitt Peak 4 meter telescope on the nights of 1998 November 30 and December 1. The 75 l mm^{-1} grating was used with the $1''.9$ slit, providing coverage of the entire K -band with a two-pixel resolution of $R = \lambda/\Delta\lambda = 300$. Wavelength calibration was performed with HeNeAr lamp spectra. LR 1 and LR 15/V410 Anon 14 were also observed at a spectral resolution of $R = 1200$ with the IR spectrometer FSpec (Williams et al. 1993) at the Multiple Mirror Telescope (MMT) on Mount Hopkins on 1997 October 14. The remaining observing and data reduction procedures for both instruments were similar to those described by Luhman et al. (1998b). I also obtained optical spectra of LR 10/V410 Anon 3, LR 13/V410 Anon 1, LR 14/V410 Anon 2, LR 15/V410 Anon 14, V410 X-ray 8b, 8d, and 8e, where the latter three stars are candidate counterparts to X-ray sources in the study of L1495 by Strom & Strom (1994). These measurements were made with the Red Channel Spectrograph at the MMT on 1997 November 27-29 and are identical to observations of stars in IC 348 by Luhman et al. (1998b) during the same nights.

2.2. Photometry

For optical imaging, I selected the regions observed by BHSM towards the L1495, B209, L1529, and L1551 dark clouds (see their Figure 1). Images of these fields were obtained with the four shooter camera at the Fred Lawrence Whipple Observatory 1.2 m telescope on 1999 October 12 and 13 under photometric conditions. The instrument contained four 2048×2048 CCDs separated by $\sim 45''$ and arranged in a 2×2 grid. After binning 2×2 during readout, the plate scale was $0''.67 \text{ pixel}^{-1}$. Two positions separated by $40''$ in right ascension and declination were observed towards L1495, B209, L1529, and contiguous north and south sections of L1551. At each position, images were obtained at I ($\lambda_{eff} \sim 8100 \text{ \AA}$) and z' ($\lambda_{eff} \sim 9100 \text{ \AA}$) with exposure times of 1 and 20 min for each filter. The images were bias subtracted, divided by dome flats, registered, and combined into one image at each band. Image coordinates and photometry were measured with DAOFIND and PHOT under the IRAF package APPHOT. Aperture photometry was extracted with a radius of four pixels. The background level was measured in an annulus around each source and subtracted from the photometry, where the inner radius of the annulus was five pixels and the width was one pixel. The photometry was calibrated in the Cousins I system through observations of standards across a range of colors (Landolt 1992). Because the I filter for these observations was similar to Cousins I , the color transformation was small. The z' filter is similar to that of the Sloan Digital Sky Survey (Fukugita et al. 1996). The z' data were calibrated by the standard star with the most neutral colors ($V - I = 0.2$) and assuming $I - z' = 0$. This crude calibration is sufficient for this study since the z' data are used only in identifying likely background stars and young low-mass candidates through the relative $I - z'$ colors. Saturation occurred near $I \sim 12.5$. The completeness limits were $I \sim 21$ and $z' \sim 19.5$ as inferred from a comparison of the data to the number of stars as a function of magnitude in the Galactic models of Bahcall & Soneira (1981). Typical photometric uncertainties are 0.04 mag at $I = 20$ and $z' = 18.5$ and 0.1 mag at $I = 21$ and $z' = 19.5$. The plate solution was derived from coordinates of sources observed in the 2MASS Spring 1999 Release Point Source Catalog that appeared in the optical images and were not saturated.

The centers and dimensions of the fields from which photometry is extracted are $(\alpha, \delta)(2000) = (4^{\text{h}}18^{\text{m}}36^{\text{s}}.65, 28^{\circ}23'30''.5)$ and $23'.42 \times 23'.42$ for L1495, $(\alpha, \delta)(2000) = (4^{\text{h}}14^{\text{m}}12^{\text{s}}.15, 28^{\circ}10'51''.5)$ and $23'.42 \times 23'.42$ for B209, $(\alpha, \delta)(2000) = (4^{\text{h}}32^{\text{m}}31^{\text{s}}.1, 24^{\circ}23'37''.5)$ and $23'.1 \times 22'.5$ for L1529, and $(\alpha, \delta)(2000) = (4^{\text{h}}31^{\text{m}}47^{\text{s}}.8, 18^{\circ}09'35''.0)$ and $23'.18 \times 46'.83$ for L1551. 2MASS photometry is currently unavailable for the northern 70% of the L1551 field (north of $\delta = 18^{\circ}00'06''.0$). Out of nearly 2000 2MASS sources within these four fields, 66 objects were not measured in the optical data because they fell within gaps between the detectors, were contaminated by bad pixels, or were not point sources (e.g., galaxies). These 2MASS sources are excluded from the study. In addition, a known asteroid that was flagged in the 2MASS database was rejected. In the areas covered by 2MASS, stars saturated in the optical data were included in the compilation of sources through their 2MASS photometry and coordinates. But in the portion of L1551 not available in 2MASS, no photometry is available for saturated optical sources, and thus they are omitted. The exceptions are

V826 Tau, XZ Tau, HL Tau, V827 Tau, V710 Tau A and B, which are young stars with previously measured photometry. Two additional young stars that fall in the L1551 field and lack 2MASS data are L1551/IRS5 and LkH α 358. Because the former is broad and nebulous in the optical data, photometry and coordinates were not measured for it in this work. For these eight stars, IR photometry is taken from Kenyon & Hartmann (1995). The recently discovered low-mass objects MHO 4, MHO 5, MHO 6, MHO 7, and MHO 9 (BHSM) lack 2MASS photometry or other previous IR data. Photometry and coordinates for spectroscopically confirmed young members within the imaged fields of Taurus are listed in Table 1. When available, the coordinates in Table 1 are those measured from the optical data. For the other stars – 2MASS sources that were saturated or too red to be detected in the optical images – the 2MASS coordinates are given.

3. Individual Source Characteristics

3.1. Spectral Types

The targets in the spectroscopic sample can be foreground stars, background stars, or young low-mass members of Taurus. Foreground M dwarfs are identified by the lack of reddening in their spectra and colors and by the strong absorption in the optical Na and K transitions (Luhman et al. 1998a, 1998b). The star LR 10/V410 Anon 3 exhibits these properties with a spectral type of M5V, which is consistent with the classification as a foreground M4.5V star by Strom & Strom (1994). Other previously known foreground M stars in L1495 include V410 Anon 12 and 17 (Strom & Strom 1994; BHSM). Note that V410 Anon 3 was mistakenly omitted as an alternate designation for LR 10 in Table 2 of LR98. In addition, LR 11 and LR 17/V410 Anon 27 are in fact the same star. As discussed by Strom & Strom (1994), V410 Anon 9 may be a field star close to and behind the L1495 cloud. It is taken as a background star in the remaining analysis. The question of membership of this star has no bearing on the analysis of the IMF because it has a reddening higher than the limit used in defining the IMF sample.

Young late-type members of Taurus are expected to have strong absorption in TiO, VO, and H₂O at optical and near-IR wavelengths. Thus, they should be easily identified through low-resolution spectroscopy from *I* through *K*. On the other hand, background stars are predominantly giants and early-type stars. These stars exhibit featureless spectra at low resolution in the optical and IR, except for giants which have strong CO absorption at 2.3 μ m. The following targets from the spectroscopic sample are classified as background stars: V410x8b (RC, C), 8d (RC), 8e (RC, LR98), LR 2 (C), LR 3/V410 Anon 19 (C), LR 4/V410 Anon 21 (C), LR 5-8 (C), LR 9/V410 Anon 26 (C), LR 12 (C), LR 13/V410 Anon 1 (RC), LR 14/V410 Anon 2 (RC), LR 15/V410 Anon14 (BHSM, RC, F), and LR 17/V410 Anon 27 (C). The classifications are from the new data with Red Channel (RC), CRSP (C), and FSpec (F) and from the previous work of BHSM and LR98.

A spectral type of K4-K5 is measured for LR 1 from the FSpec data in the manner described by LR98. This star cannot be a foreground star because of its reddened colors. It is too bright for

its spectral type to be a background star (i.e., above the main sequence), therefore it is taken as a young member of Taurus. Spectral types for LR 1 and all other known young sources within the four Taurus fields are listed in Table 1.

3.2. Extinctions

Extinctions for the known young stars in the four Taurus fields are now estimated.

In the following analysis, standard dwarf colors are taken from the compilation of Kenyon & Hartmann (1995) for types earlier than M0 and from the young disk populations described by Leggett (1992) for types of M0 and later. The IR colors from Leggett (1992) are on the CIT photometric system. Most of the IR data in Table 1 are from the 2MASS survey, where the photometric system is similar to CIT. The IR colors of the standards and the eight young stars taken from Kenyon & Hartmann (1995) are transformed from Johnson-Glass to CIT (Bessell & Brett 1988) during the analysis, although the colors of those young stars remain in Johnson-Glass in Table 1. Reddenings are calculated with the extinction law of Rieke & Lebofsky (1985).

In the common method for estimating the reddening towards a young star, a color excess is calculated by assuming the intrinsic color, typically that of a standard dwarf at the spectral type in question. To ensure that the color excess reflects only the effect of reddening, contamination from short or long wavelength excess emission is minimized by selecting colors between the R and H bands. Because $R - I$ is less susceptible to excess emission than $J - H$, the former is used for measuring reddening in this study when it is available. The $R - I$ colors of 35 stars in Table 1 are provided by BHSM, Strom & Strom (1994), and Kenyon & Hartmann (1995). The reddenings computed by BHSM for their late M objects are slightly lower than the values reported here because of the differing references for standard dwarf $R - I$ colors between the two studies. Although dwarf colors have been assumed here, the intrinsic $R - I$ colors of young stars do appear to depart from dwarf values for M4-M5 types (Luhman 1999).

Meyer, Calvet, & Hillenbrand (1997) estimated the locus of intrinsic $J - H$ and $H - K$ colors for a sample of classical T Tauri stars (CTTS) by dereddening the observed colors with the extinctions measured from $R - I$. The locus had an origin that fell near the intrinsic colors of an M0 dwarf and it extended to redder $J - H$ and $H - K$ with a well-defined slope, a behavior that was reproduced by models of star-disk systems. When the same experiment is repeated for the sources with $R - I$ in this study, the stars are distributed around the CTTS locus of Meyer et al. (1997) in a similar fashion as in Figure 4 of LR98 for L1495. However, the scatter is larger than that found by Meyer et al. (1997), probably because the sample here is not as homogeneous in spectral type or as well-studied photometrically.

To calculate reddenings for each of the 14 stars in Table 1 that has a spectral type but lacks an $R - I$ measurement, the $J - H$ and $H - K$ colors are dereddened to a CTTS locus where the origin coincides with the dwarf colors for the star’s spectral type. The locus is given the slope

measured by Meyer et al. (1997) for M0 stars, which they predicted to remain relatively constant with spectral type. This method assumes that the central stars of young mid- and late-M stars have dwarf-like $J - H$ and $H - K$ colors, which is suggested by the work of Luhman (1999). Most of the stars dereddened in this fashion have extinctions that are nearly the same as those derived by simply assuming dwarf colors without including the CTTS locus, i.e., they have little IR excess emission. An exception is PSC04154+2823, which exhibits an excess in $H - K$ that is larger than expected from a reddened CTTS. To estimate the extinction for this object, the $J - H$ color is dereddened to a value of 1.1, which is roughly the maximum intrinsic color of the CTTS locus. In the compilation of Kenyon & Hartman (1995), the binary V710 Tau ($3''24$, Leinert et al. 1993) is resolved in the IR photometry but not in the optical data. Because the intrinsic optical colors of the components probably differ significantly given their spectral types, the IR colors are used in measuring the extinctions towards each component. Reddenings and luminosities are not calculated for the three sources lacking spectral types and the class I object L1551/IRS5.

3.3. Effective Temperatures and Bolometric Luminosities

For reasons described in previous studies (e.g., Luhman 1999), I and J are the preferred bands for measuring bolometric luminosities of young low-mass stars. When J is available, the luminosities in Table 1 are computed from standard dwarf bolometric corrections (see Luhman 1999), the dereddened J -band measurements, and a distance modulus of 5.76 (Wichmann et al. 1998). For the five members that lack IR data, luminosities are estimated from the I -band photometry obtained in this study. Because HL Tau, PSC04154+2823, and MHO 1 have strong excess emission in the near-IR, the luminosities inferred from J have large uncertainties. In addition, such sources are often highly variable, as found for PSC04154+2823 when the photometry of this work and BHSM are compared ($\Delta I = 1.66$).

Spectral types of M0 and earlier are converted to effective temperatures with the dwarf temperature scale of Schmidt-Kaler (1982). For spectral types later than M0, the adopted temperature scale is that developed by Luhman (1999) for use with the evolutionary models of Baraffe et al. (1998). Detailed discussions of the temperature scales and evolutionary models for young low-mass stars are found in LR98, Luhman (1999), and Luhman et al. (2000).

4. The Taurus Stellar Population

4.1. Membership and Completeness

4.1.1. Separation of Field Stars and Candidate Low-Mass Members

To distinguish cool, low-mass cluster members from background stars in a color-magnitude diagram, the photometric bands should be selected such that the directions of decreasing mass and

increasing extinction differ as much as possible. For example, in a plot of $J - H$ versus H , members of a population will move vertically down the diagram with lower mass and cooler temperatures because the near-IR colors of most spectral types fall within a small range of values. Meanwhile, extinction moves stars down and to the right at a relatively shallow angle in this diagram. As a result, cluster members and reddened background stars are mixed together and cannot be separated with IR colors alone. However, in a color-magnitude diagram that includes at least one optical band (e.g., $R - I$, $I - z'$, $I - J$), the color increases rapidly with later spectral types and the reddening vector has a steep slope downward. In such a diagram, the intersection of reddened background stars and low-mass members is minimized, allowing for the efficient rejection of most of the field stars.

For the above reasons, BHSM used an optical color-magnitude diagram to search for new low-mass members of Taurus in fields towards L1495, B209, L1529, and L1551. At stellar masses, spectroscopy was obtained for nearly all candidate members; only a few objects near the locus of Taurus members were not observed spectroscopically. BHSM obtained spectra for all but one of the brown dwarf candidates at $I \leq 18$ in the diagram of $R - I$ versus I (their Figure 2). The object lacking a spectrum is a likely brown dwarf (see § 4.1.3) and is shown as an open triangle in the various color-color and color-magnitude diagrams. Thus, in the $I - z'$ versus I and $J - H$ versus $I - K_s$ diagrams in Figs. 1 and 2, after plotting this brown dwarf candidate and the spectroscopically confirmed members, all other stars at $I \leq 18$ can be labeled as field stars. Because the spectroscopy is not 100% complete for the candidates at stellar masses, a few of the objects taken as field stars may be young stars.

I can now use the color-color and color-magnitude diagrams presented here to separate background stars and candidate low-mass members that are beyond the sensitivity of the BHSM study ($I = 18-21$). To determine the regions in Figs. 1 and 2 where low-mass Taurus members should appear, I must plot the intrinsic colors and magnitudes expected for young brown dwarfs at masses of 0.02 and 0.08 M_\odot . The $I - z'$ colors for these masses are estimated in the following manner. The combination of the models of Baraffe et al. (1998) and the compatible temperature scale of Luhman (1999) indicate that brown dwarfs at masses of 0.02 and 0.08 M_\odot and an age of 1 Myr should have spectral types near M9 and M6.5, respectively. From the locus of reddened background stars in Figure 2, I measure a reddening slope of $E(I - K_s)/E(J - H) = 4.0$. By combining this slope with the dwarf colors of Leggett (1992) for spectral types of M9 and M6.5, I plot the reddening vectors for 0.02 and 0.08 M_\odot from $A_H = 0-1.4$ in Figure 2. The $E(I - K_s)/E(J - H)$ slope is also combined with $E(J - H) = 0.107 A_V$ (Rieke & Lebofsky 1985) and $A_{K_s} = 0.116 A_V$ (extrapolated from A_K of Rieke & Lebofsky 1985) to derive $A_I = 0.544 A_V$. After measuring a slope of $E(I - z')/E(J - H) = 0.75$ from the distribution of field stars in $I - z'$ versus $J - H$, I arrive at $E(I - z') = 0.08 A_V$. From this extinction relation and the reddenings in Table 1, the intrinsic $I - z'$ colors of the M6-M6.25 Taurus members are calculated. These dereddened $I - z'$ colors are then extrapolated to M6.5 and M9 ($I - z' = 1.6$ and 1.75) by using the variation in $I - Z$ from M6 to M9 for objects in the field and the Pleiades open cluster (Steele & Howells 2000; Zapatero

Osorio et al. 1999). The magnitudes at I for 0.02 and $0.08 M_{\odot}$ at an age of 1 Myr are calculated by combining the bolometric corrections and distance modulus from § 3.3 with the luminosities predicted by Baraffe et al. (1998). The resulting positions for these two masses are shown in Figure 1. Most stars in these Taurus fields have ages of $\lesssim 3$ Myr, with a few as old as 10 Myr (§ 4.2.1). Therefore, to obtain a census that is complete down to $0.02 M_{\odot}$, the boundary in Figure 1 used in selecting low-mass candidates must include objects at $0.02 M_{\odot}$ with ages as old as 10 Myr. From 1 to 10 Myr, the evolutionary models of Baraffe et al. (1998) and Burrows et al. (1997) predict a decrease in luminosity of 0.5 and 0.9 mag, respectively. Thus, to be conservative in the rejection of field stars, a reddening vector is placed at 1 mag below the position of $0.02 M_{\odot}$ in Figure 1; any low-mass members with masses above $0.02 M_{\odot}$ should fall above this line. The nature of stars above the reddening vector will be examined in more detail in § 4.1.3. Stars below this vector are rejected as field stars for the purposes of calculating the IMF down to $0.02 M_{\odot}$. However, substellar members of Taurus with masses of $\lesssim 0.01 M_{\odot}$ ($\gtrsim L0$) could fall below the reddening vector because the $I - z'$ color saturates at early L types (Steele & Howells 2000). As demonstrated in Figure 1, most of the targets identified as foreground and background stars through spectroscopy could have been rejected by deep I and z' photometry alone had it been available.

4.1.2. Selection of the Reddening Limit of the IMF Sample

Because the mass and reddening vectors are roughly perpendicular in a near-IR color-magnitude diagram and because all of the late-type members should have similar intrinsic IR colors, completeness in mass and reddening are readily evaluated with near-IR data. Thus, by combining the 2MASS data with the membership information from the spectroscopy and the optical color-magnitude diagrams of BHSM and this work, I can determine the optimum reddening limit for the sample used in calculating the IMF. This reddening limit will be high enough to include a large number of cluster members while low enough to achieve completeness to very low masses. In Figure 3, the near-IR color-magnitude diagram is generated from the 2MASS data for the four Taurus fields, with the exception of the portion of L1551 that was unavailable in 2MASS (see § 2.2). The membership status is established for most of the faint sources at $J - H \leq 1.5$. Because this color corresponds to a reddening of $A_H = 1.4$ for young brown dwarfs ($J - H \sim 0.65$; Luhman 1999), I select a reddening limit of $A_H \leq 1.4$ for the sample from which the IMF is computed. If a young brown dwarf with $A_H \leq 1.4$ exhibited an excess at $J - H$ arising from emitting circumstellar material, it could fall in the region of high $J - H$ in Figure 3 where membership status is uncertain for most objects. However, the fraction of stellar members that have such large excesses at $J - H$ is very small. Furthermore, the young brown dwarfs studied by Luhman (1999) in IC 348 appear to have negligible excess emission in $J - H$.

4.1.3. Any Brown Dwarfs within the Reddening Limit?

I now determine whether there are any new low-mass candidates within the reddening limit that is used for the IMF measurement. In Figs. 1-4, stars that have not been rejected as field stars in § 4.1.1 and are not known members are divided into three categories: stars detected only in the 2MASS data (no I and z'), optical sources with high reddening (high $J - H$), and optical sources with low reddening (low $J - H$). For the former sources, the membership status cannot be unambiguously determined because only IR data is available. However, this is not important for the IMF calculation because these objects are either fainter than the H magnitude of the desired completeness limit of $0.02 M_{\odot}$ or are redder than the extinction limit of $A_H \leq 1.4$, as shown in Figure 3 and discussed further in § 4.1.5. The high reddening category consists of sources that fall to the right of the $A_H \leq 1.4$ reddening vectors in Figure 3; these stars are beyond the extinction limit for the IMF and therefore are not considered further. Finally, the low reddening objects are defined as those between the $A_H \leq 1.4$ reddening vectors for 0.02 and $0.08 M_{\odot}$ or below the vector for $0.02 M_{\odot}$ in Figure 3. Because the three objects in this category are within the reddening limit of the IMF sample, their membership status must be examined to determine whether they should be added to the IMF. The brightest of these three sources is 2MASSs J0418511+281433, the brown dwarf candidate of BHSM mentioned in § 4.1.1. The 2MASS and optical photometry for this object are $H = 13.19$, $J - H = 0.71$, $H - K_s = 0.44$, $I = 16.77$, and $I - z' = 1.67$. As shown in Figure 2 of BHSM and in Figs. 1 and 2, 2MASSs J0418511+281433 has the colors and magnitudes expected for a young brown dwarf. The second brightest source is 2MASSs J0432086+242213, which has $H = 15.11$, $J - H = 1.47$, $H - K_s = 0.22$, $I = 20.61$, and $I - z' = 2.18$. This object does not have a high enough ratio of $I - K_s$ to $J - H$ to be a late-type member of Taurus, as demonstrated in Figure 2. The third object, 2MASSs J0417504+281440, has $H = 15.33$, $J - H = 1.45$, $H - K_s = 0.92$, $I = 22.31$, and $I - z' = 2.34$. This source has $J - H$ and $I - K_s$ colors that are consistent with a late M type (reddest of the three open triangles in Figure 2). However, because it falls at the detection limit in both the optical and IR data, its positions in the color-color and color-magnitude diagrams are uncertain. This source is taken to be a field star for the remainder of this work; the membership status of this one object is not important for the conclusions of this study. In summary, there is one compelling brown dwarf candidate lacking spectroscopy and within the reddening limit of $A_H \leq 1.4$ used for the IMF in L1495, B209, L1529, and the portion of L1551 currently available through 2MASS.

4.1.4. Special Considerations for L1551

For the portion of the L1551 field that is not included in the 2MASS photometry, the identification of low-mass candidates and estimation of completeness must be performed with the optical data alone. The objects in this region that are not rejected as field stars by the $I - z'$ versus I diagram are labeled with open boxes in Figure 1. Without IR data, the completeness is not assured for high reddenings at substellar masses. Therefore, rather than use a reddening limit of $A_H \leq 1.4$

to calculate the IMF as done in the other fields, a smaller range of extinctions must be considered for this part of L1551. Because 12 of the 14 known young stars in L1551 have $A_H = 0-0.5$, $A_H \leq 0.5$ is taken as the reddening limit for the calculation of the IMF in this part of L1551. For the IMF to be representative for masses of $\leq 0.02 M_\odot$, low-mass candidates must be identified down to the magnitude of a $0.02 M_\odot$ brown dwarf at an age of 10 Myr with a reddening of $A_H = 0.5$, which corresponds to $I = 20.6$. This magnitude was computed by combining the luminosities and temperatures predicted by Baraffe et al. (1998) with the temperature scale and bolometric corrections discussed in § 3.3. There is only one L1551 object above this brightness that is not rejected as a field star. In the other fields covered by 2MASS, all but one of the stars falling above the reddening vector in Figure 1 were found to be either highly reddened or a field star when the optical and IR data were combined. Thus, because it is likely that this one object in L1551 would also be rejected in the same manner if IR photometry were available, it is not considered a likely brown dwarf.

4.1.5. *The Mass Completeness of the Reddening-Limited Sample*

The reddening-limited sample described here would not be an accurate reflection of the Taurus population if the average extinctions were a function of mass, e.g., young brown dwarfs were more highly reddened than stars. In previous magnitude-limited searches for low-mass stars and brown dwarfs in star forming clusters (e.g., Luhman 1999; Wilking, Greene, & Meyer 1999) no difference in reddening characteristics has been found between the stellar and substellar members. The data in this study can be used as an additional test of whether brown dwarfs are hidden by higher amounts of extinction than the known stellar population. Most of the targets of the IR spectroscopy were selected from the imaging of LR98 towards a $10' \times 10'$ region of the L1495 dark cloud. As shown in the IR color-magnitude diagram for this area in Figure 4, no low-mass members are found at a dereddened magnitude of $H > 10.5-13$ in a sample where the membership status is complete to large reddenings ($A_V \lesssim 20$). Although this test suffers from poor number statistics, it is consistent with the result from studies of other young regions that a reddening-limited measurement produces a representative IMF down to substellar masses.

The sample selected for measuring the IMF is defined by $A_H \leq 0.5$ for a portion of L1551 and $A_H \leq 1.4$ elsewhere. As discussed in the previous two sections, out of the objects with optical photometry, there is one likely brown dwarf within these reddening limits and lacking spectroscopy; it will be added to the IMF in § 4.2.1. For stars with only IR photometry, membership cannot be determined. However, none of these stars are within the reddening ($A_H \leq 1.4$) and mass ($\leq 0.02 M_\odot$) limits for ages of ≤ 1 Myr, as shown in Figure 3. Because the 1 and 3 Myr isochrones are nearly coincident at $0.02 M_\odot$, this statement holds for an age limit of 3 Myr as well. The sample is incomplete only for objects that are simultaneously old (10 Myr) and at the reddening and mass limits. Because such objects occupy a tiny fraction of the mass-reddening-age phase space and because most members of these Taurus fields have ages of ≤ 3 Myr (see Figure 5), this incompleteness is negligible. Because there remain ~ 5 candidate members at stellar masses that

lack spectra in the color-magnitude diagram of BHSM, the completeness for brown dwarfs above $0.02 M_{\odot}$ is as good or better than that for stars. Thus, although the census of members may not be 100% complete in any mass interval, it is not biased against brown dwarfs and is representative down to a mass of $0.02 M_{\odot}$.

4.2. The Initial Mass Function

4.2.1. *Taurus*

In the Hertzsprung-Russell (H-R) diagram in Figure 5, the models of Baraffe et al. (1998) are plotted with the Taurus members from Table 1, with the exception of L1551/IRS5, the three objects with unknown spectral types, and the two earliest stars. These models are used to infer masses for individual sources from their estimated temperatures and luminosities. For stars in the reddening-limited sample that are above the solar mass track of Baraffe et al. (1998), the prescription of Luhman et al. (2000) is followed; the two stars are placed in one mass bin from $\log M = -0.05$ to 0.35 (0.89 - $2.2 M_{\odot}$). 2MASSs J0418511+281433 is the one likely Taurus member that lacks a measured spectral type and is within the reddening limit of the IMF sample. If an age of 1 Myr is assumed for this object, the optical and IR photometry (§ 4.1.3) imply a mass of $\sim 0.03 M_{\odot}$ with the models of Baraffe et al. (1998). Because the masses of many of the low-mass sources in the Trapezium IMF of Luhman et al. (2000) were derived through photometry alone, they used the bin size of $\Delta \log M = 0.4$ at all masses. For all but one of the sources in the Taurus IMF, on the other hand, more precise masses are inferred through spectroscopy and placement on the H-R diagram, thus, smaller mass bins of $\Delta \log M = 0.2$ are used below $\log M = -0.05$. The IMF from the reddening-limited sample for the four Taurus fields contains 40 sources and is presented in Figure 6.

4.2.2. *Comparison of Taurus and Clusters*

Luhman et al. (2000) found that the stellar IMFs in the young clusters IC 348, ρ Oph, and the Trapezium are consistent with the same mass function, while modest variations in the substellar IMFs are possible. Because of the superior number statistics in the Trapezium sample, that IMF is taken to represent star forming clusters in the following comparison between Taurus and clusters.

For a meaningful comparison of the IMFs in Taurus and the Trapezium, it is important that the IMFs have been constructed from samples that are physically equivalent and relatively primordial. Thus, the minimum separations of objects in the two samples should correspond to the same physical scale and should be less than the distance at which disruption through dynamical interactions is significant. These criteria have been satisfied fairly well; the IMFs for the Trapezium and Taurus consist of sources with separations greater than $0''.7$ and $2''$, respectively, which are equal physical

distances. Furthermore, these separations are less than the length scales in the Trapezium ($\sim 1''$) and Taurus ($\sim 90''$) that mark the transitions from the binary regime to large-scale clustering (Gomez et al. 1993; Larson 1995; Simon 1997; Nakajima et al. 1998; Bate, Clarke, & McCaughrean 1998), which in turn should be less than the maximum binary separations (Bate et al. 1998).

Because the samples in Taurus and the Trapezium have been designed to be comparable in their binarity and because the same techniques were employed in estimating the masses for each population, the IMFs for the two regions can be reliably compared. In addition, the optimum reddening limit for each sample is $A_H = 1.4$ (except for L1551), making the two IMFs particularly suitable for comparison. The methods of these studies should also produce reasonably accurate measurements of the IMFs in each region (see Luhman et al. 2000).

The IMFs for Taurus and the Trapezium are plotted together in Figure 6, where both mass functions are representative down to $0.02 M_\odot$. The Trapezium IMF has been normalized to the Taurus data between 0.1 and $1 M_\odot$. Over this mass range, the two mass functions are consistent with the same shape; a peak at $0.6-1 M_\odot$ followed by slight decline and flattening down to $0.1 M_\odot$. However, below $0.1 M_\odot$ the two IMFs differ greatly. If the IMF in Taurus were the same as that in the Trapezium, 12.8 ± 1.8 brown dwarfs ($> 0.02 M_\odot$) are expected in the former, but only one is found. Relative to the Trapezium, Taurus exhibits a deficit of higher mass stars as well. At $1-2 M_\odot$ the renormalized Trapezium IMF contains 7.8 ± 1.4 stars while the Taurus sample has only 2 stars. Neither IMF is characterized by a log-normal distribution.

The deficit of brown dwarfs in Taurus relative to the Trapezium motivates searches for variations in substellar mass functions in regions of intermediate stellar densities. For instance, the number statistics of the substellar census in IC 348 (Luhman et al. 1998b; Luhman 1999) and ρ Oph (Luhman & Rieke 1999; Wilking et al. 1999) can be improved to determine whether they differ from the Trapezium at a significant level.

The significant number of brown dwarfs in the field (Reid et al. 1999) and the scarcity of them in Taurus combined with the similarity of the IMFs in star forming clusters, young open clusters, and the field (Luhman et al. 2000) are convincing evidence that the field is populated by stars born in clusters rather than isolated regions (Lada, Strom, & Myers 1993).

4.2.3. *Implications for Theories of the IMF*

Luhman et al. (2000) compared predictions of theories of the IMF to the shape of the low-mass IMF, its approximate invariance at stellar masses among IC 348, ρ Oph, and the Trapezium, and the minimum mass observed for isolated objects ($\sim 0.01 M_\odot$), possibly below the deuterium burning mass limit ($0.013-0.015 M_\odot$, Burrows et al. 1997). In addition, while similarities between the mass functions of pre-stellar clumps and the stellar IMF have recently been reported and suggested as evidence that the process of fragmentation determines the masses of stars (Motte, André, & Neri 1998; Testi & Sargent 1998), Luhman et al. (2000) found that a closer comparison

of these pre-stellar mass functions to accurate IMFs recently derived for star forming regions is not yet conclusive. I now include the implications of the new IMF for Taurus and its behavior relative to the mass function for the Trapezium.

The high-mass IMF in Taurus is first considered. Elmegreen (1997, 1999, 2000) contended that differences in measurements of IMF slopes may be statistical fluctuations rather than true variations in the IMF. Regions with fewer high mass stars simply do not have enough members to populate the mass function to high masses. He points to the agreement between cluster IMFs and the integrated galaxy IMF as supporting evidence. However, it is clear from the work presented here and by Luhman et al. (2000) that star forming clusters rather than sparse regions like Taurus are responsible for the Galactic field population. Thus, a true deficit of high-mass stars in Taurus would not be reflected in the Galactic IMF. Indeed, a comparison of Taurus and the Trapezium suggests that the lack of high-mass stars is not because of poor sampling of the IMF, although the statistical significance of this result should be improved through an expansion of this work to include a larger fraction of the Taurus population. Elmegreen does refer to possible exceptions to his model, such as the extreme field in the LMC and Milky Way (Massey et al. 1995), where the high-mass IMFs are much steeper than those in the Galactic and cluster IMFs. In fact, Elmegreen (1999) briefly refers to a scenario in which a low-density star forming region like Taurus could produce fewer high-mass stars.

The predictions of individual theories are now compared to the low-mass IMFs in Taurus and the Trapezium.

While wind-limited accretion models for the IMF (Adams & Fatuzzo 1996) can account for the value of the low-mass cutoff in Taurus, they do not explain the change in the minimum mass from Taurus to the Trapezium, the very low value of the cutoff in the Trapezium, or the deficit of high-mass stars in Taurus. Furthermore, if the IMF is determined by a large number of variables, a log-normal form is predicted for the IMF, which is not observed in either region.

Elmegreen (1997, 1999) presented a model where the IMF is controlled by fragmentation from hierarchical clouds modulated by the Jeans condition. The shape of the IMF at intermediate masses in Taurus and the Trapezium – a power law slope followed by a turnover and flattening – is reproduced by this model (and many others; Scalo 1999). Both the turnover mass and the minimum mass should be reflections of the Jeans mass, thus they should change together from one region to another. However, this is not the case in the Taurus and the Trapezium populations, which exhibit the same turnover masses of $\sim 0.8 M_{\odot}$ but very different low-mass cutoffs of $\lesssim 0.01 M_{\odot}$ and $\sim 0.08 M_{\odot}$, respectively.

Theories of the IMF that rely on interactions of cores or protostars (Lejeune & Bastien 1986; Murray & Lin 1996; Price & Podsiadlowski 1995; Bonnell et al. 1997) have difficulty in explaining the similarity of the turnover masses in the Trapezium and Taurus, where the stellar densities differ by three orders of magnitude. Dynamical interactions and competitive accretion between protostellar cores were also important in shaping the IMF in numerical modeling of the gravitational

collapse and fragmentation of a dense cloud core by Klessen, Burkert, & Matthew (1998). The predicted IMF exhibited a log-normal form that was centered at a mass described by the product of the Jeans mass of the system and the star forming efficiency. As demonstrated here and by Luhman et al. (2000), the IMF is not characterized by a log-normal function, with the possible exception of that in globular clusters.

Any theory of the IMF must explain the differences in the frequencies of brown dwarfs and (more tentatively) of high-mass stars between Taurus and young clusters. One property that varies dramatically from Taurus to star forming clusters is the level of turbulence observed in cloud cores (Myers 1998), which may be the ultimate origin of these IMF variations. For instance, it is possible that both the growth and the fragmentation of pre-stellar cores are enhanced in more turbulent environments, which could broaden the IMF in a dense cluster relative to that in an isolated region (Myers 2000b). Further modeling of the formation of stellar clusters within turbulent dense cores (Klessen et al. 1998; Myers 1998, 2000a) may help explain the observed behavior of the low-mass IMF.

5. Conclusion

An IMF that is representative for masses down to $0.02 M_{\odot}$ has been measured for fields near the L1495, B209, L1529, and L1551 dark clouds in the Taurus star forming region. These data and similar studies of star forming clusters provide powerful constraints on theories of star formation.

The observations for star forming clusters as summarized by Luhman et al. (2000) are first reviewed:

1. Above $0.1 M_{\odot}$, the IMFs in the core of IC 348, the cloud core of ρ Oph, and the Trapezium Cluster are indistinguishable within the counting uncertainties.
2. Below $0.1 M_{\odot}$, the IMFs in the three clusters are roughly similar, although the statistical uncertainties in the data for ρ Oph and IC 348 allow for modest variations.
3. Data for the Trapezium, young open clusters, and the field are consistent with the same IMF, which differs from the IMF that characterizes globular clusters (Paresce & De Marchi 2000).
4. The IMF for young clusters and the field is flat or slowly rising from the substellar regime to $\sim 0.6 M_{\odot}$ and then rolls over into a power law that continues from $\sim 1 M_{\odot}$ to higher masses with a slope similar to or somewhat larger than the Salpeter value of 1.35; it cannot be described by a log-normal function.
5. In the Trapezium, the IMF is flat down to $0.02 M_{\odot}$ or lower and contains a population of ~ 50 likely brown dwarfs.
6. The least massive objects observed in the Trapezium appear to have masses of $\sim 0.01 M_{\odot}$.

The new conclusions provided by this study of Taurus are as follows:

1. Above $1 M_{\odot}$, the fields of Taurus in this study have proportionately fewer stars than the Trapezium at a modest level of significance.
2. From 0.1 - $1 M_{\odot}$, the IMF in Taurus matches that of the Trapezium; both regions have a turnover mass near $\sim 0.8 M_{\odot}$ and a slow decline and flattening to lower masses.
3. Below $0.1 M_{\odot}$, there is a significant deficit of objects in Taurus relative to the Trapezium. If the Trapezium IMF is normalized to the Taurus IMF by the numbers of objects between 0.1 - $1 M_{\odot}$, then 12.8 ± 1.8 brown dwarfs at $> 0.02 M_{\odot}$ are present in the Trapezium where one is found in the Taurus fields.
4. In summary, if the Trapezium IMF is steepened above $1 M_{\odot}$ and suppressed below $0.1 M_{\odot}$, then the result is the IMF for Taurus; it cannot be described by a log-normal function.

I am grateful to F. Allard, I. Baraffe, and F. D’Antona for access to their most recent calculations. Discussions with L. Hartmann, G. Rieke, J. Stauffer and, in particular, P. Myers are appreciated. I also thank C. Briceño for providing details concerning his published work. K. L. was funded by a postdoctoral fellowship at the Harvard-Smithsonian Center for Astrophysics. This publication makes use of data products from the Two Micron All Sky Survey, which is a joint project of the University of Massachusetts and the Infrared Processing and Analysis Center, funded by the National Aeronautics and Space Administration and the National Science Foundation.

REFERENCES

- Adams, F. C., & Fatuzzo, M. 1996, *ApJ*, 464, 256
- Bahcall, J. N., & Soneira, R. M. 1981, *ApJS*, 47, 357
- Baraffe, I., Chabrier, G., Allard, F., & Hauschildt, P. H. 1998, *A&A*, 337, 403
- Barrado y Navascués, D., Stauffer, J. R., Bouvier, J., Martín, E. L. 2000, *ApJ*, submitted
- Bate, M. R., Clarke, C. J., & McCaughrean, M. J. 1998, *MNRAS*, 297, 1163
- Bessell, M. S., & Brett, J. M. 1988, *PASP*, 100, 1134
- Bonnell, I. A., Bate, M. R., Clarke, C. J., & Pringle, J. E. 1997, *MNRAS*, 285, 201
- Bouvier, J., Stauffer, J. R., Martín, E. L., Barrado y Navascués, D., Wallace, B., & Bejar, V. J. S. 1998, *A&A*, 336, 490
- Briceño, C., Hartmann, L., Stauffer, J., & Martín, E. L., 1998, *AJ*, 115, 2074 (BHSM)
- Burrows, A., Marley, M., Hubbard, W. B., Lunine, J. I., Guillot, T., Saumon, D., Freedman, R., Sudarsky, D., & Sharp, C. 1997, *ApJ*, 491, 856

- Elmegreen, B. G. 1997, *ApJ*, 486, 944
- Elmegreen, B. G. 1999, *ApJ*, 515, 323
- Elmegreen, B. G. 2000, in *Star Formation from the Small to the Large Scale*, eds. F. Favata, A. A. Kaas, & A. Wilson (ESA Publications Division at ESTEC, Noordwijk, The Netherlands), ESA SP-445, in press
- Fukugita, M., Ichikawa, T., Gunn, J. E., Doi, M., Shimasaku, K., & Schneider, D. P. 1996, *AJ*, 111, 1748
- Gomez, M., Hartmann, L., Kenyon, S. J., & Hewett, R. 1993, *AJ*, 105, 1927
- Herbig, G. H., & Bell, K. R. 1988, *Lick Obs. Bull. Ser.*, No. 1111
- Hillenbrand, L. A., & Carpenter, J. M. 2000, *ApJ*, in press
- Kenyon, S. J., & Hartmann, L. 1995, *ApJS*, 101, 117
- Kenyon, S. J., Brown, D. I., Tout, C. A., & Berlind, P. 1998, *AJ*, 115, 2491
- Kirkpatrick, J. D., et al. 1999, *ApJ*, 519, 802
- Lada, E. A., Strom, K. M., & Myers, P. C. 1993, in *Protostars and Planets III*, eds. E. H. Levy, J. I. Lunine, & M. S. Matthews (University of Arizona Press, Tucson), 245
- Landolt, A. U. 1992, *AJ*, 104, 340
- Larson, R. B. 1995, *MNRAS*, 272, 213
- Leggett, S. K. 1992, *ApJS*, 82, 351
- Leinert, Ch, Zinnecker, H., Weitzel, N., Christou, J., Ridgway, S. T., Jameson, R., Haas, M., & Lenzen, R. 1993, *A&A*, 278, 129
- Lejeune, C., & Bastien, P. 1986, *ApJ*, 309, 167
- Luhman, K. L. 1999, *ApJ*, 525, 466
- Luhman, K. L., Briceño, C., Rieke, G. H., & Hartmann, L. W. 1998a, *ApJ*, 493, 909
- Luhman, K. L., & Rieke, G. H. 1998, *ApJ*, 497, 354 (LR98)
- Luhman, K. L., & Rieke, G. H. 1999, *ApJ*, 525, 440
- Luhman, K. L., Rieke, G. H., Lada, C. J., & Lada, E. A. 1998b, *ApJ*, 508, 347
- Luhman, K. L., Rieke, G. H., Young, E. T., Cotera, A. S., Chen, H., Rieke, M. J., Schneider, G., & Thompson, R. 2000, *ApJ*, in press
- Massey, P., Lang, C. C., Degioia-Eastwood, K., & Garmany, C. D. 1995, *ApJ*, 438, 188
- Meyer, M. R., Calvet, N., & Hillenbrand, L. A. 1997, *AJ*, 114, 288
- Motte, F., André, P., & Neri, R. 1998, *A&A*, 336, 150
- Murray, S. J., & Lin, D. N. C. 1996, *ApJ*, 467, 728
- Myers, P. C. 1998, *ApJ*, 496, L109

- Myers, P. C. 2000a, *ApJ*, 530, 119
- Myers, P. C. 2000b, in preparation
- Nakajima, Y., Tachihara, K., Hanawa, T., & Nakano, M. 1998, *ApJ*, 497, 721
- Paresce, F., & De Marchi, G. 2000, *ApJ*, 534, 870
- Price, N. M., & Podsiadlowski, Ph. 1995, *MNRAS*, 273, 1041
- Reid, I. N., et al. 1999, *ApJ*, 521, 613
- Rieke, G. H., & Lebofsky, M. J. 1985, *ApJ*, 288, 618
- Scalo, J. 1999, in *The Birth of Galaxies*, ed B. Guiderdoni et al. (Gif-sur-Yvette, Editions Frontières), in press
- Schmidt-Kaler, T. 1982, in *Landolt-Bornstein, Group VI, Vol. 2*, ed. K.-H. Hellwege (Berlin: Springer), 454
- Simon, M. 1997, *ApJ*, 482, L81
- Silk, J. 1995, *ApJ*, 438, 41
- Steele, I. A., & Howells, L. 2000, *MNRAS*, 313, 43
- Strom, K. M., & Strom, S. E. 1994, *ApJ*, 424, 237
- Testi, L., & Sargent, A. I. 1998, *ApJ*, 508, L91
- Wichmann, R., Bastian, U., Krautter, J., Jankovics, I., & Ruciński, S. M., 1998, *MNRAS*, 301, L39
- Wilking, B. A., Greene, T. P., & Meyer, M. R. 1999, *AJ*, 117, 469
- Williams, D., Thompson, C. L., Rieke, G. H., & Montgomery, E. F. 1993, *ProcSPIE*, 1308, 482
- Zapatero Osorio, M. R., Rebolo, R., Martín, E. L., Hodgkin, S. T., Cossburn, M. R., Magazzù, A., Steele, I. A., & Jameson, R. F. 1999, *A&AS*, 134, 537

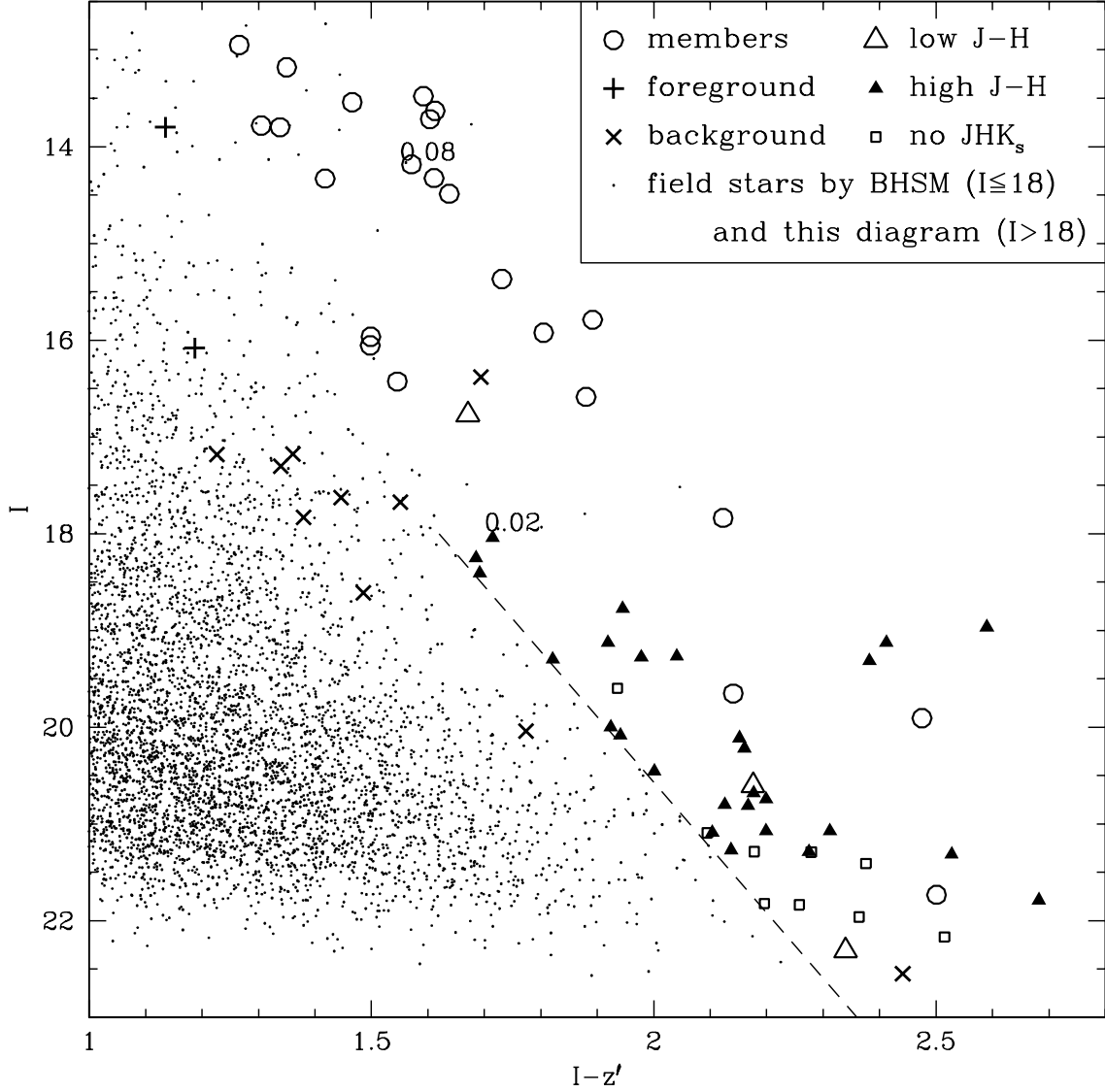


Fig. 1.— $I - z'$ vs. I for fields surrounding the L1495, B209, L1529, and L1551 dark clouds in the Taurus star forming region. Stars that have been spectroscopically identified as Taurus members, foreground stars, and background stars are indicated. At $I \leq 18$, all other stars except for one object (open triangle) are field stars by the spectroscopy and $R - I$ vs. I diagram of BHSM. At $I > 18$, Taurus members with masses of $\geq 0.02 M_{\odot}$ and ages of ≤ 10 Myr are expected to fall above the dashed reddening vector. Any stars below this line are labeled as field stars. The stars above the reddening vector are categorized as having low $J - H$, high $J - H$, or no JHK_s photometry. Objects with low $J - H$ are within the reddening limit of $A_H \leq 1.4$ that defines the sample from which the IMF is calculated. Sources without JHK_s photometry are within the portion of the L1551 not currently available in 2MASS. The unreddened positions of 0.08 ($\sim M6.5$) and 0.02 M_{\odot} ($\sim M9$) are shown for an age of 1 Myr (Baraffe et al. 1998).

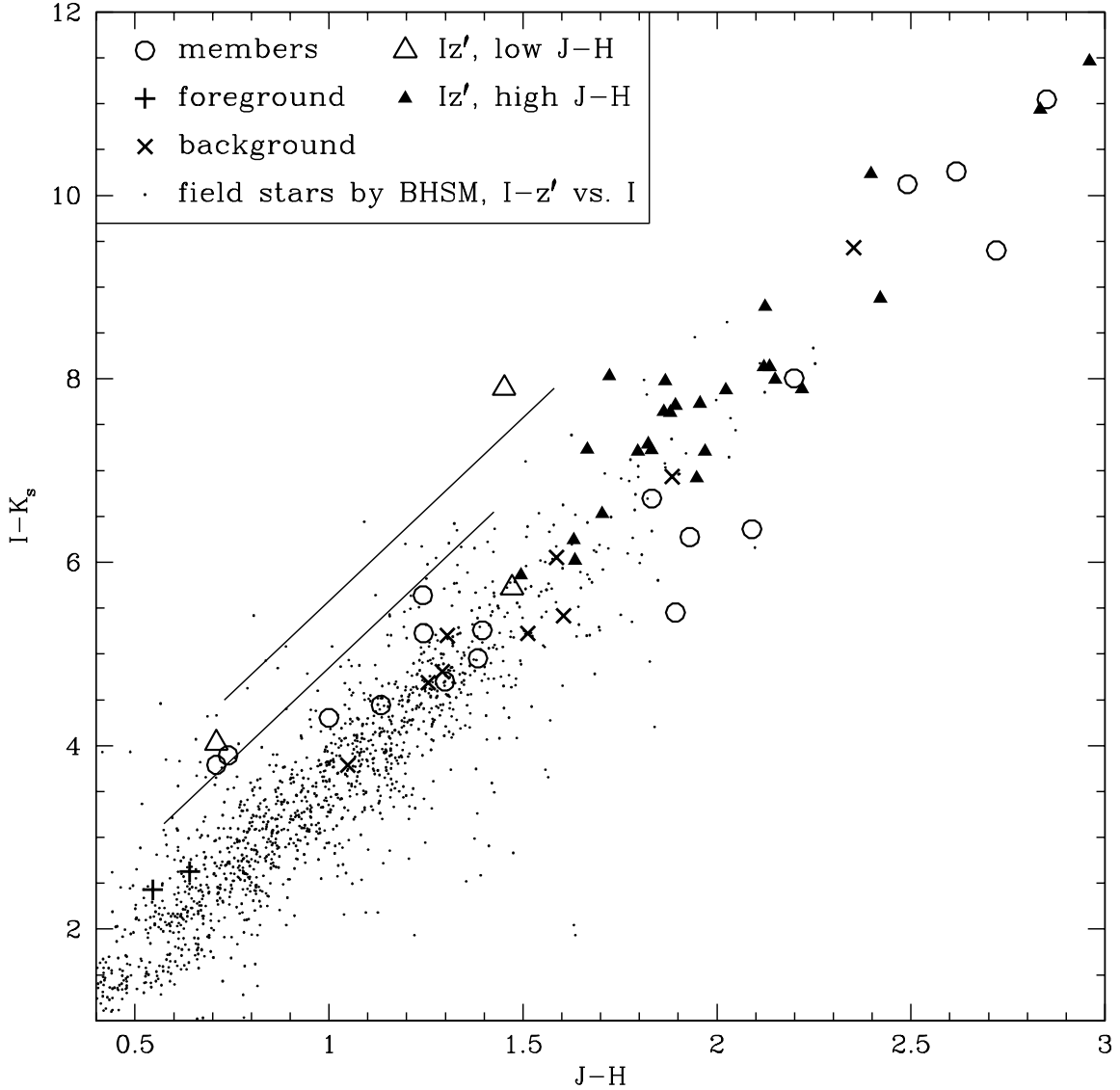


Fig. 2.— $J - H$ vs. $I - K_s$ for fields surrounding the L1495, B209, L1529, and L1551 dark clouds in the Taurus star forming region. Stars that have been spectroscopically identified as Taurus members, foreground stars, and background stars are indicated. Objects that are field stars by the I and z' data in Figure 1 and by the spectroscopy and RI data of BISM are also shown. The remaining stars that are not rejected as field stars through those means are categorized as having low $J - H$ or high $J - H$. Objects with low $J - H$ are within the reddening limit of $A_H \leq 1.4$ that defines the sample from which the IMF is calculated. The lower and upper lines represent the reddening vectors from $A_H = 0-1.4$ for spectral types of M6.5 and M9 (Leggett 1992), which correspond to 0.08 and 0.02 M_\odot for an age of 1 Myr (Baraffe et al. 1998).

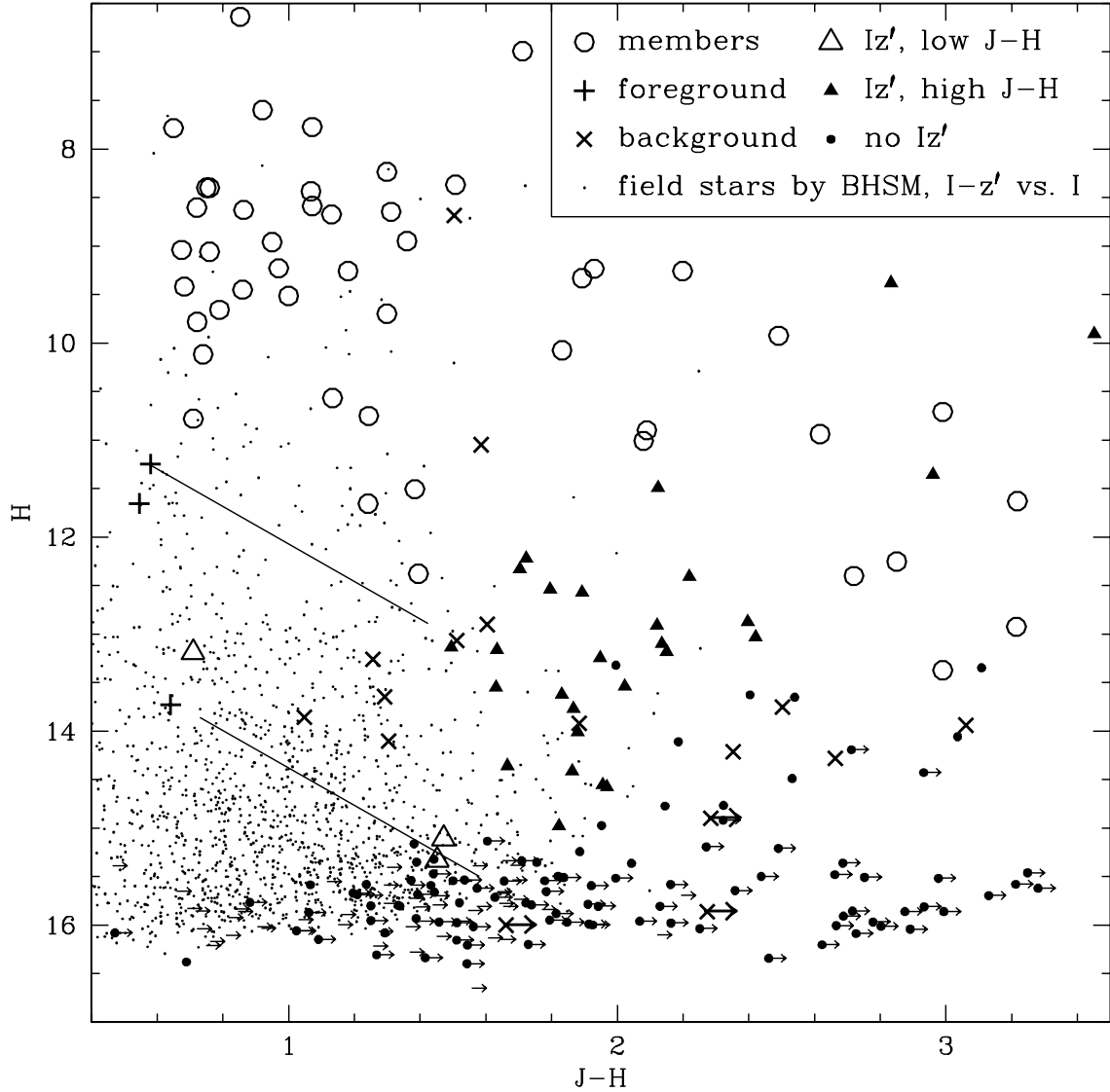


Fig. 3.— $J - H$ vs. H from the 2MASS survey for fields surrounding the L1495, B209, L1529, and L1551 dark clouds in the Taurus star forming region, with the exception of portion of L1551 not currently available in 2MASS. Stars that have been spectroscopically identified as Taurus members, foreground stars, and background stars are indicated. Objects that are field stars by the I and z' data in Figure 1 and by the spectroscopy and RI data of BHSM are also shown. The remaining stars that are not rejected as field stars through those means are categorized as having low $J - H$, high $J - H$, or no I and z' data. Objects with low $J - H$ are within the reddening limit of $A_H \leq 1.4$ that defines the sample from which the IMF is calculated. The upper and lower lines represent the reddening vectors from $A_H = 0-1.4$ for 0.08 ($\sim M_{6.5}$) and $0.02 M_{\odot}$ ($\sim M_9$) for an age of 1 Myr (Baraffe et al. 1998).

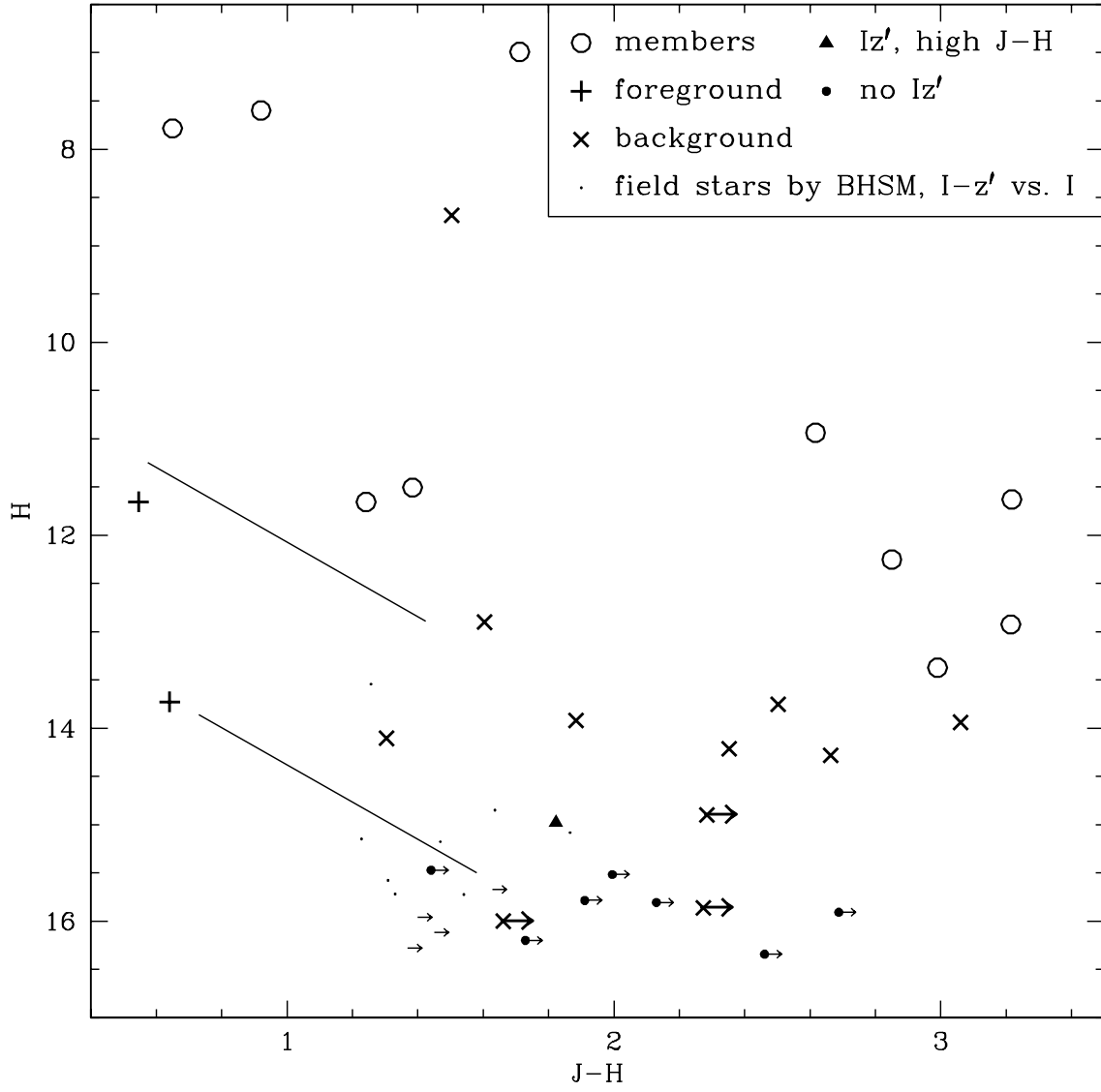


Fig. 4.— Same as Figure 3, but restricted to the $10' \times 10'$ region of the L1495 dark cloud imaged by LR98.

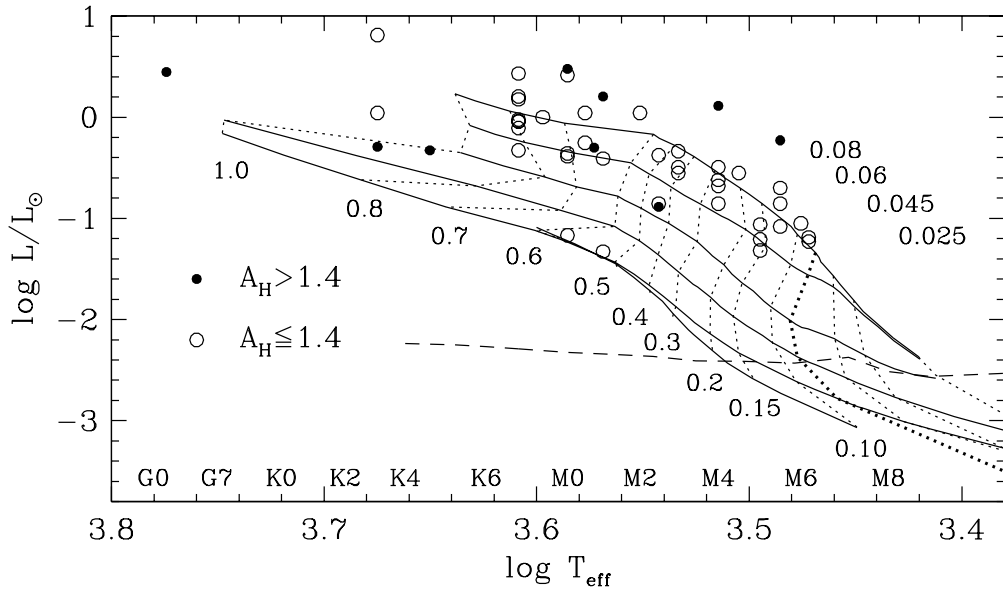


Fig. 5.— H-R diagram for fields surrounding the L1495, B209, L1529, and L1551 dark clouds in the Taurus star forming region. The theoretical evolutionary models of Baraffe et al. (1998) are shown, where the horizontal solid lines are isochrones representing ages of 1, 3, 10, 30, and 100 Myr and the main sequence, from top to bottom. The dashed line in the H-R diagram represents a dereddened magnitude of $H = 14$. The M spectral types have been converted to effective temperatures with a scale that is compatible with these evolutionary models (Luhman 1999), which is intermediate between the scales for M dwarfs and giants.

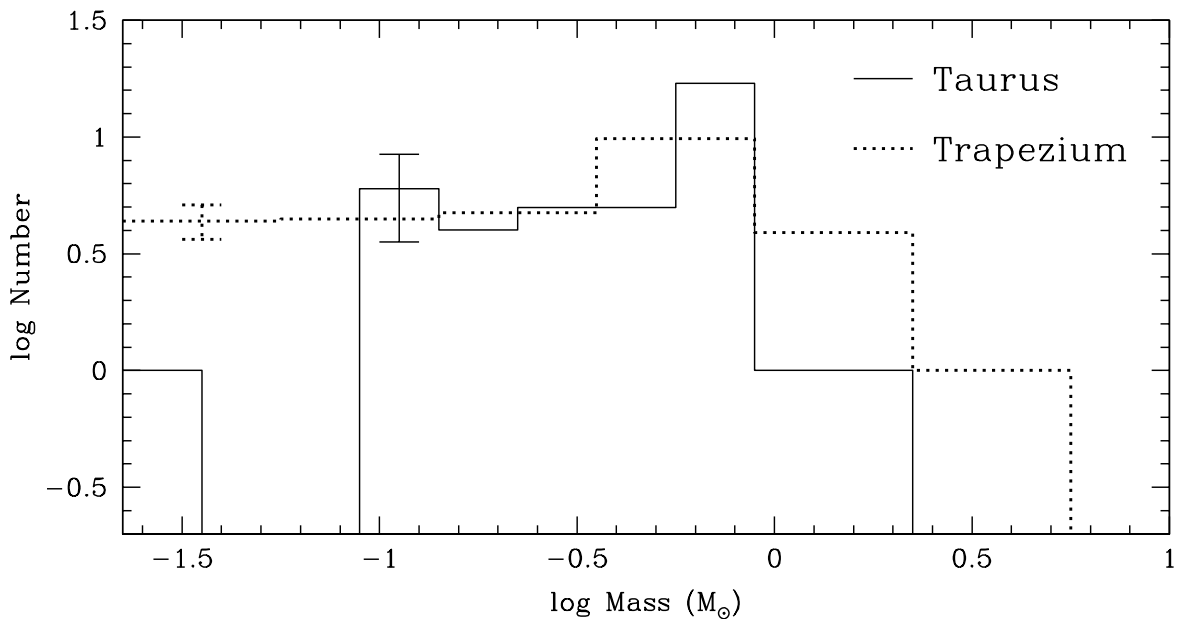


Fig. 6.— IMFs for reddening-limited samples in the Taurus star forming region and the Trapezium Cluster (Luhman et al. 2000) as inferred from the evolutionary models of Baraffe et al. (1998). The IMF for the Trapezium has been renormalized for comparison to the Taurus data. Both IMFs are representative over the entire mass range shown. The mass bins for the Trapezium IMF are twice the size of the ones for the Taurus data (§ 4.2.1).

TABLE 1
YOUNG STARS IN SELECTED FIELDS OF TAURUS

ID ^a	$\alpha(2000)$	$\delta(2000)$	Optical Type ^b	IR Type ^b	Adopt	T_{eff}^c	A_H	L_{bol}	$R - I$	$I - z'$	I	$J - H$	$H - K_s$	K_s	in IMF?
Anon 1	4 13 27.21	28 16 24.9	M0(1)	...	M0	3850	0.64	2.6	1.07	0.36	7.41	yes
V773 Tau	4 14 12.91	28 12 12.4	K3(1)	...	K3	4730	0.29	6.5	0.85	0.85	0.43	6.21	yes
FM Tau	4 14 13.57	28 12 49.3	M0(1)	...	M0	3850	0.34	0.44	1.16	0.86	0.70	8.75	yes
CW Tau	4 14 17.00	28 10 57.8	K3(1)	...	K3	4730	0.34	1.1	0.91	1.30	1.12	7.12	yes
CIDA-1	4 14 17.61	28 06 09.8	C(1)	1.42	14.33	1.13	0.68	9.89	no
MHO 1	4 14 26.27	28 06 03.2	M2.5(3)	...	M2.5	3488	~ 1.0	~ 0.14	2.40	2.12	17.84	2.49	2.21	7.71	yes
MHO 2	4 14 26.40	28 05 59.7	M2.5(3)	...	M2.5	3488	1.15	0.42	2.60	1.89	15.79	2.20	1.47	7.78	yes
MHO 3	4 14 30.55	28 05 14.6	K7(3)	...	K7	4060	1.33	0.91	2.36	1.64	14.49	1.93	1.02	8.21	yes
FO Tau	4 14 49.28	28 12 30.4	M2(1),M2(2)	...	M2	3560	0.61	1.1	1.07	0.48	8.11	yes
CIDA-2	4 15 05.16	28 08 46.1	M4.5(1)	...	M4.5	3198	0.10	0.28	0.68	0.34	9.08	yes
V410 X-ray 1	4 17 49.65	28 29 36.4	M4(2)	...	M4	3270	0.16	0.14	1.79	1.30	13.78	1.30	0.62	9.08	yes
V410 X-ray 3	4 18 07.98	28 26 03.7	M6(2),5,3)	M4.5-M8.5(4)	M6	2990	0.14	0.089	2.27	1.57	14.18	0.71	0.39	10.39	yes
V410 Anon 13	4 18 17.11	28 28 41.8	M5(2),M5-M7(3)	K2-K6(4)	M5	3125	0.67	0.048	2.61	1.88	16.59	1.24	0.71	10.95	yes
V410 Anon 24	4 18 22.41	28 24 37.3	...	F9-G3(4)	G1	5945	4.18	2.8	...	2.50	21.73	2.85	1.57	10.68	no
V410 Anon 25	4 18 29.09	28 26 19.1	...	K7-M3(4)	M1	3705	4.06	1.6	3.22	1.76	0.87	9.87	no
V410 Tau	4 18 31.10	28 27 16.1	K3(1),K7(2)	...	K7	4060	0.00	1.5	0.70	0.65	0.17	7.61	yes
DD Tau	4 18 31.13	28 16 28.9	M1(1),M4(2)	...	M4	3270	0.00	0.32	1.44	1.13	0.81	7.87	yes
CZ Tau	4 18 31.58	28 16 58.5	M1.5(1),M3(2)	...	M3	3415	0.32	0.28	1.73	0.72	0.45	9.34	yes
PSC 04154+2823	4 18 32.05	28 31 15.3	...	M0.5-M4.5(4)	M2.5	3488	~ 2.6	~ 0.13	...	2.14	19.65	2.72	2.15	10.25	no
V410 X-ray 2	4 18 34.44	28 30 30.2	...	K6-M2(4)	M0	3850	3.74	3.0	2.99	1.55	9.16	no
V410 X-ray 4	4 18 40.23	28 24 24.4	...	M3-M5(4)	M4	3270	3.28	1.3	...	2.48	19.91	2.62	1.29	9.64	no
V892 Tau	4 18 40.61	28 19 15.4	A6(1),B9(2)	...	B9	10500	1.48	77	1.71	1.71	1.24	5.76	no
LR 1	4 18 41.33	28 27 24.9	...	K4-K5(8)	K4.5	4470	3.97	0.47	3.21	1.94	10.98	no
V410 X-ray 7	4 18 42.49	28 18 49.7	M1(2),M0.5(3)	...	M0.75	3741	1.45	0.50	2.62	1.80	15.92	1.83	0.85	9.23	no
V410 Anon 20	4 18 45.05	28 20 52.9	...	K1-K5(4)	K3	4730	4.08	0.51	2.99	1.46	11.92	no
Hubble 4	4 18 47.03	28 20 07.3	K7(1),K7(2)	...	K7	4060	0.42	2.7	1.27	0.92	0.32	7.28	yes
CoKu Tau/1	4 18 51.48	28 20 26.5	M0(7),M2(2)	...	M0	3850	0.68	0.068	1.57	1.50	15.96	1.38	0.50	11.01	yes
PSC 04158+2805	4 18 58.14	28 12 23.7	...	K7-M3(4)	M1	3705	1.02	0.047	2.14	1.55	16.43	1.39	1.21	11.17	yes
V410 X-ray 6	4 19 01.10	28 19 42.1	M5(2),M5.5(6)	M2.5-M6.5(4)	M5.5	3058	0.11	0.20	2.08	1.59	13.48	1.00	0.34	9.18	yes
V410 X-ray 5a	4 19 01.98	28 22 33.3	M5(2),M5.5(6,3)	M3-M5(4)	M5.5	3058	0.45	0.083	2.49	1.73	15.37	1.24	0.61	10.14	yes
FQ Tau	4 19 12.81	28 29 33.1	M2(1),M4(2)	...	M4	3270	0.10	0.21	1.72	0.79	0.36	9.30	yes
V819 Tau	4 19 26.26	28 26 14.3	K7(1),K7(2)	...	K7	4060	0.30	0.91	1.12	0.86	0.23	8.40	yes
MHO 9	4 31 15.94	18 20 04.7	M4(3)	...	M4	3270	0.39	0.24	2.07	1.27	12.95	yes
MHO 4	4 31 24.08	18 00 21.6	M6-M6.5(3)	...	M6.25	2965	0.17	0.059	2.36	1.61	14.32	yes
L1551/IRS5	4 31 34.1	18 08 04	G-K(1)	2.08	1.74	9.27	no
LkH α 358	4 31 36.27	18 13 40.9	M5.5(1)	...	M5.5	3058	2.38	0.59	...	1.49	16.05	2.09	1.21	9.69	no
HL Tau	4 31 38.4	18 13 59	K7(1)	...	M0	3850	~ 0.3	~ 0.41	1.11	1.36	1.61	7.34	yes
XZ Tau	4 31 40.0	18 13 58	M3(1)	...	M3	3415	0.05	0.32	1.41	0.95	0.91	8.05	yes
HK Tau	4 31 50.55	24 24 18.6	M0.5(1)	...	M0.5	3778	0.60	0.56	1.56	1.18	0.67	8.59	yes
V710 Tau A	4 31 57.7	18 21 37	M1(1)	...	M1	3705	0.00	0.39	0.76	0.37	8.69	yes
V710 Tau B	4 31 57.7	18 21 37	M3(1)	...	M3	3415	0.47	0.46	0.97	0.41	8.82	yes
L1551-51	4 32 09.29	17 57 23.1	K7(1)	...	K7	4060	0.00	0.47	0.70	0.67	0.19	8.85	yes
V827 Tau	4 32 14.5	18 20 15	K7(1)	...	K8	3955	0.20	1.0	0.99	0.76	0.21	8.19	yes
Haro 6-13	4 32 15.43	24 29 00.0	C(1)	1.46	13.54	1.89	1.24	8.09	no
V826 Tau	4 32 15.8	18 01 39	K7(1)	...	K7	4060	0.12	0.95	0.90	0.75	0.15	8.25	yes
MHO 5	4 32 16.02	18 12 43.4	M6-M6.5(3)	...	M6.25	2965	0.02	0.065	2.18	1.61	13.72	yes
V928 Tau	4 32 18.88	24 22 27.4	M0.5(1)	...	M0.5	3778	0.45	1.1	1.38	1.07	0.35	8.09	yes
MHO 6	4 32 22.10	18 27 35.7	M5(3)	...	M5	3125	0.15	0.062	1.98	1.34	13.80	yes
MHO 7	4 32 26.27	18 27 45.2	M5(3)	...	M5	3125	0.07	0.087	1.89	1.35	13.18	yes
FY Tau	4 32 30.59	24 19 57.3	K7(1)	...	K7	4060	0.95	1.6	1.31	0.64	8.01	yes
FZ Tau	4 32 31.78	24 20 03.0	C(1)	1.51	1.06	7.31	no
MHO 8	4 33 01.99	24 21 00.1	M5.5(3)	...	M5.5	3058	0.11	0.14	2.08	1.61	13.63	0.74	0.38	9.74	yes
V830 Tau	4 33 10.04	24 33 43.4	K7(1)	...	K7	4060	0.08	0.78	0.86	0.72	0.18	8.42	yes

^a Designations are from Briceño et al. 1998 (MHO), Luhman & Rieke 1998 (LR), Strom & Strom 1994 (V410 X-ray, V410 Anon), and references within Kenyon & Hartmann 1995.

^b 1=Kenyon & Hartmann 1995 and references therein, 2=Strom & Strom 1994, 3=Briceño et al. 1998, 4=Luhman & Rieke 1998, 5=Luhman et al. 1998a, 6=Luhman 1999, 7=Kenyon et al. 1998, 8=this work.

^c Intermediate temperature scale of Luhman 1999.

NOTE.— JHK_s data are from the 2MASS survey when available. For L1551/IRS5, V826 Tau, XZ Tau, HL Tau, V827 Tau, V710 Tau A, V710 Tau B, and LkH α 358, JHK data are from Kenyon & Hartmann 1995. $R - I$ data are from Briceño et al. 1998, Strom & Strom 1994, and Kenyon & Hartmann 1995. I and $I - z'$ are from this work. Most coordinates are from the 2MASS survey or are measured from the I images, where the plate solutions were derived using 2MASS sources. The coordinates listed with lower precision are taken from Herbig & Bell 1988. Sources without optical data are saturated or not detected. Sources without IR data are within a portion of the L1551 field that is not currently available through 2MASS.